Healthcare Technology Letters

WILEY

The Institution of Engineering and Technology

LETTER OPEN ACCESS

Augmented Reality With Dynamic Anatomy Modelling for Knee Arthroscopy

Deokgi Jeung[1,2] | Hyun-Joo Lee[3,4] | Hee-June Kim[3,4] | Hyunseok Choi[5] | Jaesung Hong[1,6]

[1]Department of Robotics and Mechatronics Engineering, DGIST, Daegu, South Korea | [2]Department of Robot Applications, Korea Institute of Machinery and Materials, Daegu, South Korea | [3]Department of Orthopaedic Surgery, School of Medicine, Kyungpook National University, Kyungpook National University Hospital, Daegu, South Korea | [4]Medical Device and Robot Institute, Kyungpook National University, Daegu, South Korea | [5]DIGITRACK Inc., Daegu, South Korea | [6]R&D Center, A4LAB Inc., Daegu, South Korea

Correspondence: Jaesung Hong (jhong@a4lab.co.kr)

Received: 23 October 2025 | **Accepted:** 5 November 2025

ABSTRACT

Research on augmented reality (AR) for knee arthroscopy has not adequately focused on knee flexion during surgery. To overcome major AR errors caused by knee movement, this study presents an association model between the finite-element models of the knee surface and bones to enable dynamic anatomy modelling. The association model allows the displacement of the knee surface elements and the reaction force of the bone elements to interact with each other. During knee flexion, the real-time shape of the knee is captured with a colour and depth camera, and the association model deforms accordingly from the extension to the flexion state. The proposed model was evaluated using computed tomography data from the knees of six participants. The results showed that the association model successfully compensates for the movement of the femur and tibia within an error margin of only 3.85 mm around the drilling area. The proposed model could therefore enable effective AR-based surgical navigation during knee surgeries.

1 | Introduction

Minimally invasive knee arthroscopy is beneficial for small incisions and rapid patient recovery. However, a study that investigated over 90,000 knee arthroscopy cases reported a total complication rate of 4.7%, with surgical complications being the most common [1]. In particular, the complication rates for posterior cruciate ligament (PCL) and anterior cruciate ligament (ACL) reconstruction were 20.1% and 9.0%, respectively. These high complication rates results from the difficulties in performing precise femoral and tibial tunnel drilling, a critical procedure for connecting artificial ligaments between the femur and tibia [2]. For ACL reconstruction with independent or transtibial femoral tunnel drilling techniques, drilling errors range from 3 to 12 mm [3–6]. Our study aims to enhance drilling accuracy in ACL and PCL reconstructions via augmented reality (AR)-based surgical navigation to guide the surgical instrument to the preoperatively determined drilling positions.

In ACL and PCL reconstruction, preoperative computed tomography (CT) or magnetic resonance (MR) scans are acquired to identify the femoral and tibial footprints and create three-dimensional (3D) virtual knee models. However, CT or MR is typically performed with the knee in the extension state, whereas surgery is performed with the knee in the flexion state to facilitate the entry of drilling instruments. Thus, using a virtual knee model reconstructed from preoperative CT or MR leads to significant AR errors. In previous studies on surgical navigation for joint surgeries, invasive markers have been fixed to the bone to reduce AR errors due to anatomical changes [7–12]. However, such

Abbreviations: ACL, anterior cruciate ligament; AR, augmented reality; CT, computed tomography; FEM, finite-element method; fps, frames per second; LCL, lateral collateral ligament; MR, magnetic resonance; MCL, medial collateral ligament; PCL, posterior cruciate ligament; RGBD, red-green-blue-depth; 3D, three-dimensional; TRE, target registration error.

methods cause damage to the bone that does not typically occur in standard arthroscopy, thereby contradicting the principle of minimally invasive arthroscopy.

Recently, some studies have introduced AR in knee arthroscopy without invasive markers. Ma et al. [13] implemented simultaneous localization and mapping algorithm in the operating room by attaching a stereo camera and an inertial sensor to the rear of the arthroscope, enabling real-time tracking of the arthroscope. Shu et al. [14] reconstructed dense 3D maps of the internal knee structure using a monocular depth estimation and simultaneous localization and mapping algorithm, and were reported to achieve high registration accuracy. Wang et al. [15] utilized the built-in object tracking capability of a head-mounted display to eliminate the need for invasive markers in navigation for ACL reconstruction. Despite these advances, all of the above methods did not consider the knee flexion or anatomical structure changes during surgery. Chen et al. [16] proposed a tissue properties-based model deformation method to update knee movements in AR during surgery. However, this approach requires manual selection of more than four anatomical points in the arthroscopic view for each knee movement, which is inconvenient and interferes with surgical procedures.

In this study, we visualized real-time knee flexion by analysing the relationship between the knee surface and bones using the proposed association model, which is based on the finite-element method (FEM). The knee surface and bone models consist of isotropic linear elastic hexahedral and tetrahedral finite elements, respectively. These finite elements exchange displacement and force information, allowing for efficient association model. During surgery, the extension state of the association model is deformed to the flexion state using data from a red-green-blue-depth (RGBD) camera as a constraint.

Recently, finite-element models of joint tissues such as cartilage, meniscus, ligaments, tendons, and muscles have been proposed [17]. While these models simulate the operation of individual tissues realistically, no study has yet considered the entire knee joint motion. In the field of laparoscopy, some researchers have proposed FEM-based simulation [18–20], where internal structures such as vessels deform according to the surface deformation of the organ. These simulations have shown close agreement with actual abdominal organ deformations, thus providing the theoretical basis for our association model. However, unlike vessels, the femur and tibia are hard tissues and are anatomically distinct. To the best of our knowledge, no study has defined the association between the finite elements of the knee surface (soft tissue) and the bone (hard tissue). To validate our method, we used in vivo knee CT data from six participants, acquired in both the extension and flexion states.

2 | Methods

2.1 | CT Scan and Finite-Element Model Construction

CT scans of six male participants (two with left and four with right knees) were acquired in both the extension and flexion states. The data acquisition process was approved by our institution's ethical committee (IRB No. DGIST_20201103_HR_100_01). All participants written consent before the CT scan. In the extension state, a CT scan was acquired with the participant lying in a supine position. In the flexion state, since the knee could not fit into the CT machine in the supine position, the scan was performed with the participant in the left lateral decubitus position. To avoid surface deformations caused by pressure unrelated to knee flexion, the right knee joint was slightly lifted off the table (Figure 1). The average weight of the participants was 72.3 ±7.5 kg. Each extension-state scan was used as the preoperative image, and the flexion-state scan was used as the reference to evaluate the proposed association model. The DICOM images were segmented and transformed into 3D virtual models using 3D Slicer (https://www.slicer.org) [21].

We constructed individual finite-element models of the knee surface, femur and tibia based on the virtual models in the extension state. For the femur and tibia, we used the following form of the tetrahedral co-rotational finite-element [22] methods:

$$F = K \cdot (\mathbf{x} - \mathbf{x}_0) \rightarrow F = RK \cdot \left(R^{-1}\mathbf{x} - \mathbf{x}_0\right) \quad (1)$$

In the equation, F represents the force applied by the deformed element to its sampling points, and K represents the stiffness matrix. $\mathbf{x}$ and $\mathbf{x}_0$ are the current and initial positions, respectively. Matrix R encodes the rotation of a local frame with respect to its initial orientation and is updated at each simulation step. The co-rotational method separately calculates the deformation of linear elastic elements under rigid rotational and stretching motion, preventing the growth artefact typically seen when simulating large rotational motion with a general linear method. Due to the significant rotational motion between the femur and tibia during flexion, the use of co-rotational elements is essential. We selected the QR decomposition-based approach [23] among various co-rotational methods [24, 25] due to its higher computational efficiency.

As the number of elements increases, each simulation step requires more computational time. Therefore, we reconstructed the surface mesh of the femur and tibia with edge lengths of 20 mm to reduce the number of elements. Next, the interior of the femur and tibia were filled with tetrahedral elements using the finite-element mesh generator Gmsh (www.gmsh.info). Consequently, each participant's femur and tibia models comprised approximately 400 to 700 elements. The Young's modulus and Poisson's ratio of the bones were set to 1500 MPa and 0.3, respectively, based on a previous study [26].

For the knee surface, hexahedral elements [27] were used instead of tetrahedral element as they enhance computational efficiency by offering easier control over the number of elements. The knee surface model was composed of 7 (width) × 7 (length) × 300 (height) elements. For the interpolation between the knee surface model and the hexahedral elements, the natural coordinate system was used for simplified computation. The relationship between world and natural coordinates was defined using the Jacobian operator. As with the femur and tibia, linear elasticity was assumed, and the QR decomposition-based co-rotational approach was applied. Non-linear elasticity was not considered because it reduces real-time performance, requiring the model's stiffness matrix to be updated at every simulation

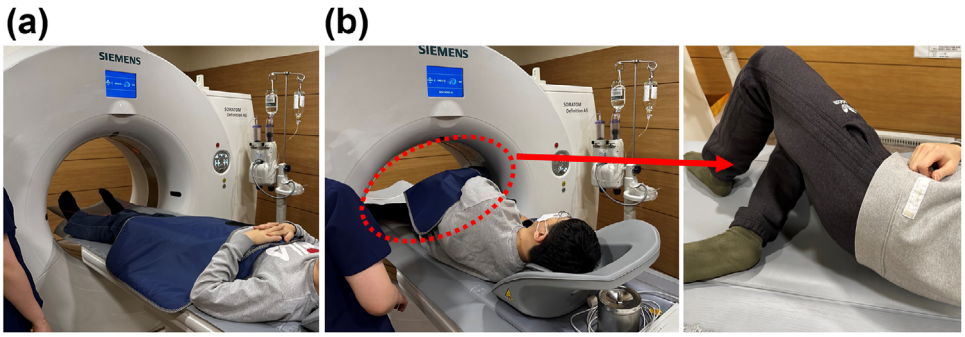

FIGURE 1 | CT scan environment of the knee. (a) Extension state. (b) Flexion state.

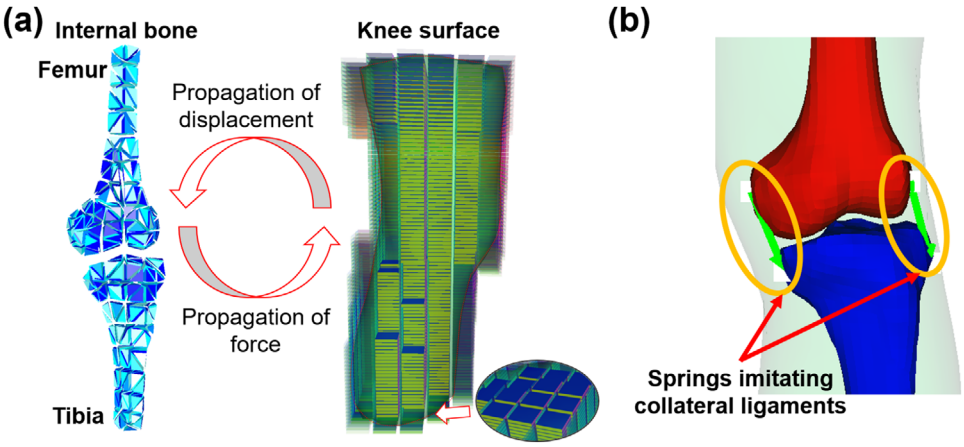

FIGURE 2 | Association model between knee surface and bones. (a) The finite-element models of the knee surface and bones exchange displacement and reaction force information with each other. (b) Collateral ligaments are integrated into the association model.

step. The Young's modulus and Poisson's ratio were empirically set to 1 MPa and 0.3, respectively, due to the mixed properties of diverse soft tissues.

2.2 | Association Model for Dynamic Anatomy

The association model maps the motion of the knee bones according to the deformation of the surface (Figure 2). To implement the association model, we advanced the previous deformable simulation method used in the liver [18–20] to accommodate our situation. Before deformation, each vertex of the tetrahedral elements of the bone model was mapped through interpolation from the surrounding vertices of the hexahedral element of the surface model. To balance modelling accuracy and computational efficiency, we assumed that the knee bones and surrounding soft tissue are strictly connected, no relative motion occurs, and the mapping relationship remains constant. In each simulation step, external forces move the hexahedral elements, and the pre-defined mapping relationship propagates the corresponding displacement to the internal tetrahedral elements of the bone. Consequently, the elastic reaction forces generated by the displacement of the tetrahedral elements are inversely propagated to the surrounding hexahedral elements (Figure 2a). In addition, hierarchical bounding volume-based collision control [28] was used to prevent overlap between the bone models. Since the femur and tibia do not make direct contact and are separated by soft tissues, collision forces are generated when the models are within 10 mm of each other.

The lateral collateral ligament (LCL) and medial collateral ligament (MCL) in the knee prevent sudden movements of the femur and tibia during flexion. The LCL resists medially directed forces that tend to push the knee outward. In contrast, MCL resists laterally directed forces that tend to push the knee inward. The proposed association model contains two first-order polynomial springs to replicate the function of the LCL and MCL (Figure 2b). Two springs are used to prevent sudden movements of the femur and tibia during deformable simulations, which may be caused by unintended inward or outward forces. The attachment position of the springs was determined by an expert orthopaedic surgeon based on the extension-state CT scans. For the best simulation results, the stiffness constant of the springs was empirically set to 1000 N/mm and their initial length was set to the ligament length in the extension state.

2.3 | Knee Flexion Simulation With Association Model

Figure 3 illustrates the association model-based deformation and the real-time AR visualization process. The 3D depth information of the knee surface was segmented from the RGBD camera data using the segment anything model (SAM, Meta AI, USA). For

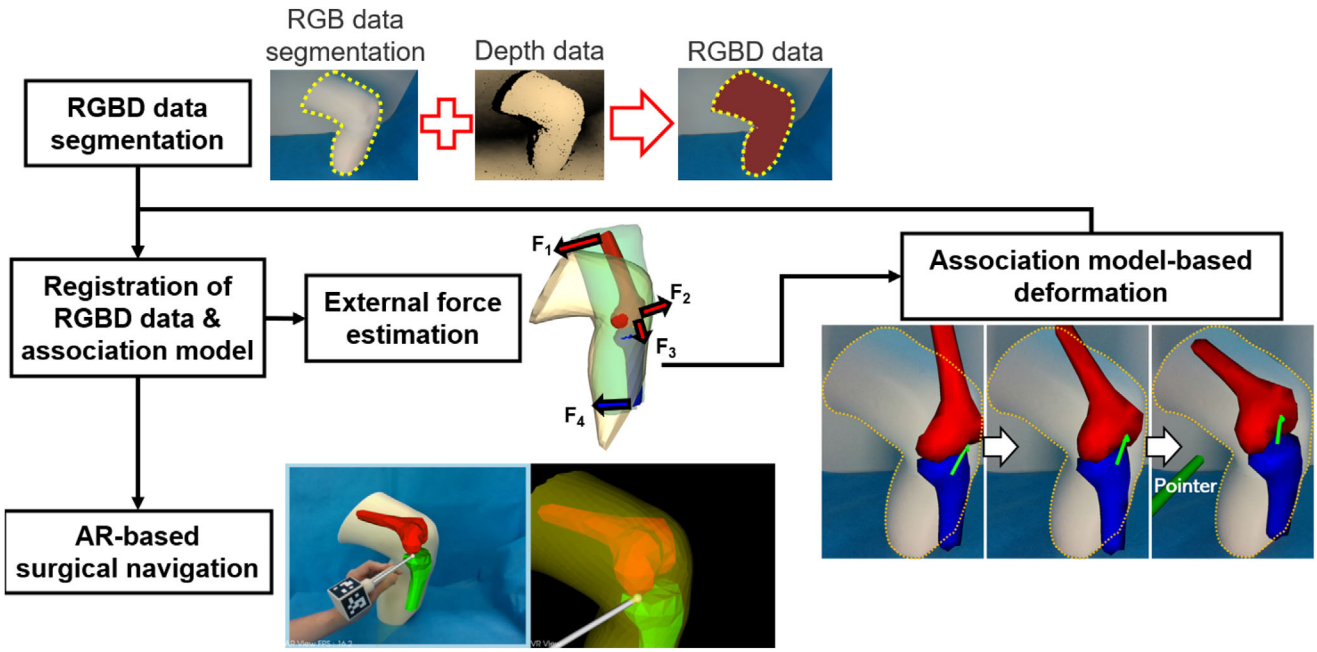

FIGURE 3 | Overall process of association model-based deformation and real-time AR visualization.

the initial registration between the segmented 3D depth information and the association model's surface, we used the iterative closest point algorithm [29]. Based on the registration result, the magnitude and direction of the external forces were estimated. During deformation, the association model was overlayed on the RGBD camera view to obtain the AR-based surgical navigation [30, 31]. The ArUco marker [32] and the OpenCV (https://opencv.org/) library were utilized to track the real-time pose of the surgical instrument. ArUco markers are widely adopted in surgical navigation systems and have been reported to provide reliable tracking performance in clinical environments [33, 34].

We defined two types of external forces for deforming the association model: bone force and surface force. Initially, only the bone force was applied to roughly align the femur and tibia in the direction of the knee flexion state. The direction of each bone force was determined by performing principal component analysis on the 3D points of the femur and tibia models. Specifically, forces F1, F2 and F3 were applied to the femur, targeting the end of the shaft and intercondylar fossa. F1 and F2 have the opposite directions. Force F4 was applied to the end of the tibia's shaft. The magnitudes of F1, F2, F3 and F4 were set as 9000, 23,000, 3000 and 6000 N, respectively.

After the angle between the femur and tibia was reduced to less than 100°, the surface forces were applied to the association model for fine deformation. These forces targeted the nearest point pairs between the knee surface model and the segmented 3D depth information, provided that the distance between the point pairs was within a predefined reference distance. In the proposed method, we used a single RGBD camera, which allowed us to capture only one side of the knee surface. In the absence of a reference distance, the opposite side of the knee surface model, which lacks a corresponding depth map, tends to be pulled towards the observed surface by surface forces. This distortion can lead to instability and eventual divergence in the deformable simulation. During fine deformation, if more than half the points on the knee surface model were within the reference distance, the distance was reduced by 0.1 mm in the next simulation step. Otherwise, it was increased by 0.1 mm for more active deformation. The initial reference distance was set as 10 mm, with maximum and minimum limits of 10 and 1 mm, respectively.

We used the following implicit form of Euler's method to solve the dynamic equilibrium equation for the deformation of the finite-element models [22]:

$$x^{(i+1)} = x^i + \Delta t\, v^{(i+1)} \tag{2}$$

$$Mv^{(i+1)} = Mv^i + \Delta t\left(-Cv^{(i+1)} - F\left(x^{(i+1)} - x_0\right) + f_{\text{ext}}^{(i+1)}\right) \tag{3}$$

In the equations, x, v, i and Δt represent the element position, element velocity, current simulation step and unit time step (0.05 s), respectively. F denotes the internal elastic forces, calculated as the product of the stiffness matrix and the deformed position of the element. f_{ext} and M represent the external forces and mass matrix, respectively. The implicit form of Euler's method is essential for accurate deformable simulation because it enables larger time steps and provides stability when dealing with stiff equations that may arise in the explicit form. To solve the dynamic equilibrium equation, we used the SOFA framework [35], an open-source library which supports the development of FEM-based medical applications. Finally, using the mapping function between the simulation and visualization models, which is supported by the SOFA framework, a dense bone model can be visualized instead of the sparse finite element bone model.

3 | Experiments and Results

Two experiments were conducted to evaluate the proposed association model. First, we created a virtual flexion-state knee model

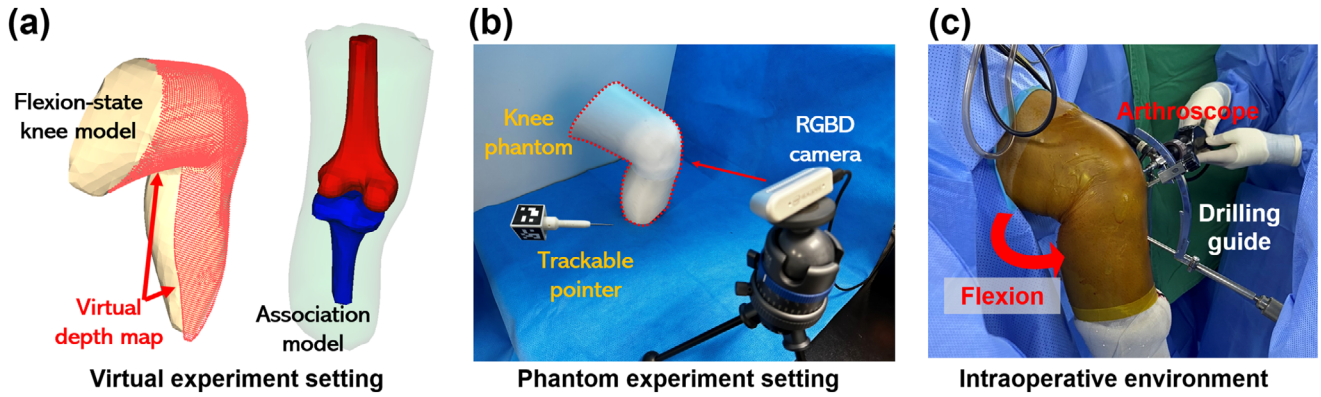

FIGURE 4 | Experimental environments.

TABLE 1 | Target point errors for knee CT data.

Participant	1(L)	2(L)	3(R)	4(R)	5(R)	6(R)
Femur	4.22 ± 1.18	5.19 ± 2.28	3.65 ± 1.19	4.51 ± 1.86	5.29 ± 1.42	6.42 ± 2.02
Tibia	4.06 ± 0.83	4.69 ± 1.42	4.70 ± 0.32	7.37 ± 1.27	5.78 ± 1.28	4.09 ± 1.02

Note: Values are expressed as mean ± standard deviation (mm).

and a corresponding virtual depth map using the flexion-state knee CT scans to evaluate the positional accuracy of the femur and tibia simulated using the association model (Figure 4a). The virtual depth map represents the 3D depth expected to be obtained from the RGBD camera. The association model, initially in the extension state, was deformed into the estimated flexion state with the virtual depth map as a constraint. The target point error was defined as the Euclidean distance between the real and estimated flexion-state knee bones. The target points are surface points on the epiphysis of the bone model, representing the target drilling areas in ACL and PCL reconstruction. The process of identifying target points is as follows. First, the reconstructed points of the femur and tibia models in the extension state were labelled based on their z-axis values. Then, using the iterative closest point algorithm, the transformation matrix between the extension and real flexion states was computed for each bone. The target points in the real flexion state were then determined by applying the corresponding transformation matrix. Finally, a surface distance map, which depicts the distance to the target point in colour, was drawn. The surface distance map represents the surface distance error between the bones in the real flexion-state model obtained from CT and those estimated by the dynamic anatomy modelling and simulation process. This visualization directly evaluates how accurately the proposed dynamic anatomy model reproduces the actual intraoperative bone positions during knee flexion.

For the second experiment, the target registration error (TRE) [31] was measured in a phantom experiment environment to evaluate the accuracy of AR-based surgical navigation (Figure 4b). A knee phantom was printed in 3D based on the flexion-state CT scans. A RealSense RGBD camera (D435i, Intel, USA) was used and configured to operate at a resolution of 1280×720 with 30 frames per second (fps). The RGBD camera was mounted approximately 30–40 cm above the phantom, capturing the knee from a slightly oblique angle, in accordance with the usage guidelines described in previous research [36]. Figure 4c illustrates the intraoperative environment and was taken from a position where an RGBD camera could be placed without hindering the surgeon's access to the operating site. The phantom experiment setup was designed to replicate this same camera position and viewing angle.

The RGBD camera trackable pointer was utilized as the surgical instrument. The pointer was designed with a hexahedral structure mounted 150 mm behind the tip, with a 40 × 40 mm marker attached to each face. The transformation between the marker coordinate system and the pointer tip was obtained from the 3D model used in the design. When the pointer tip was repeatedly positioned on a specific point of interest, the variance of the measured positions was found to be 1.23 mm. After the deformation of the association model was completed, the corresponding point in the virtual bone model needed to be selected when the point of interest on the phantom's bone was identified using a trackable pointer. Finally, four artificial landmarks were placed around the drilling area of the femur and tibia to measure the TRE.

Table 1 shows the knee flexion compensation results from the association model. The mean target point errors were 4.88 mm for the femur and 5.12 mm for the tibia. When limiting the error measurement to the ligament footprint, the errors were reduced to 3.81 mm for the femur and 3.89 mm for the tibia. Figure 5 shows the surface distance map of the target point error between the real and estimated flexion-state knee bones. In each subfigure, the yellow arrow and the red (or blue) bone model shown in the bottom right corner represent the field of view. The bright areas represent large target point errors (blue dotted circles). The drilling areas for ACL (red circles) and PCL (yellow circles) reconstruction, such as footprint and

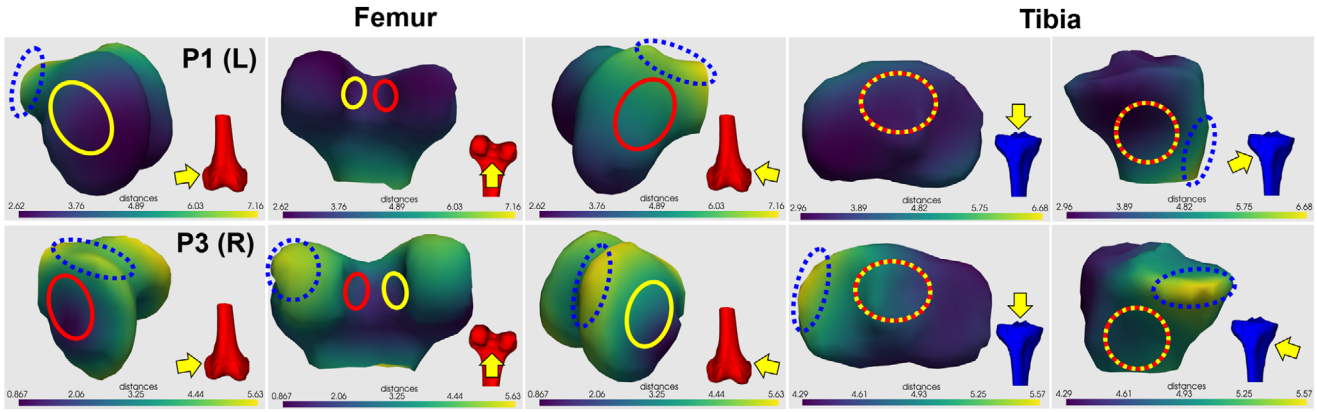

FIGURE 5 | Surface distance map for data of participants 1 (left knee) and 3 (right knee).

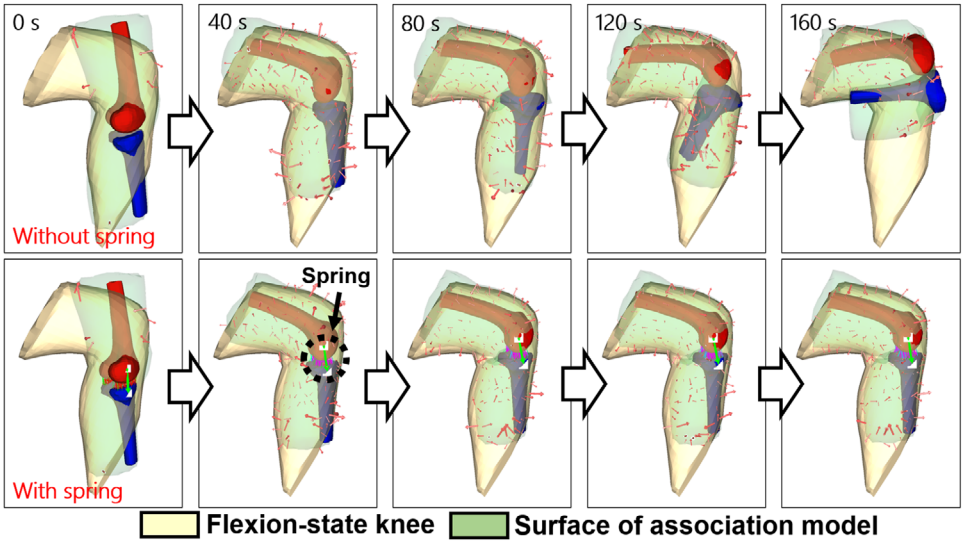

FIGURE 6 | Deformation from extension to estimated flexion state with and without spring.

epicondyle, exhibited smaller target point errors compared with the surrounding ends of the epiphysis.

Figure 6 demonstrates the deformation of the association model from the extension to the estimated flexion state, both with and without the springs. Without the springs, the model diverges into an abnormal shape over time due to the tibia's excessive outward or inward rotational motion. However, with the springs, the model stably converges to the estimated flexion state and maintains its shape over time. For the AR-based surgical navigation, the femur, tibia, drilling guidance and trackable pointer position were overlaid (Figure 3). The association model deformed to the estimated flexion state in about 60 s. Thereafter, the TREs were 4.21 mm for the femur and 3.93 mm for the tibia. The proposed AR system had an update speed of more than 9 fps during the experiment.

4 | Discussion and Conclusion

We developed a real-time dynamic anatomy model to simulate flexion during knee arthroscopy. Using the dynamic anatomy model, our method focuses on accurately visualizing the positions of the femur, tibia and surgical instrument. In ACL reconstruction, drilling errors range from 3 to 12 mm [3–6]. By comparison, the error of the proposed model for the drilling area is slightly above 3 mm, a level attainable by expert surgeons. However, identifying anatomical landmarks, such as the native ligament footprint in ACL and PCL reconstruction is difficult due to the narrow arthroscopic view. In such situations, the proposed AR-based surgical navigation assists novice surgeons in achieving drilling accuracy comparable to that of expert surgeons. In addition, some ACL reconstructions require drilling more than three times to connect two strands of the artificial ligament, which increases the risk of surgical complications. Since inappropriate drilling positions are a major cause of surgical failure in ACL reconstruction [2], the proposed AR-based navigation technique should be beneficial.

In ACL and PCL reconstruction, the positions of the native ligament footprints where the drill is inserted are determined by observing anatomical landmarks through arthroscopic imaging. However, the drill exits on the lateral or medial epicondyles are determined by the surgeon's palpation. This poses a risk of the drilling direction deviating from the preoperative plan and damaging femoral structures. The proposed AR technique depicts

the entire epiphysis and the surgical instrument position in real time, helping prevent these complications. According to a recent study, the minimum safe distance between the femoral tunnel outlet and lateral femoral structures in ACL reconstruction is 8.46 mm [37]; the proposed method satisfies this condition while offering an additional margin.

Regarding the applicability of the proposed system, a recent review paper on navigation technology for ACL reconstruction [38] reported that the use of surgical navigation can improve bone tunnel positioning accuracy and reduce the learning curve for arthroscopic surgery. Since our proposed system implements AR-based surgical navigation without invasive markers and compensates for intraoperative knee movement, it is expected to leverage these reported benefits while further improving usability compared to existing ACL navigation technologies.

Creating a digital twin of the knee joint that encompasses all individual tissues requires significant computational resources, and real-time deformation is impossible. Moreover, users must specify the physical parameters for all tissues. The proposed model simplifies the knee joint components into bones and surfaces, minimizing manual adjustment and allowing real-time responses to changes in the knee angle during surgery. Despite its simplified structure, the proposed model achieves high accuracy in AR, meeting the clinical standards. This facilitates the implementation of an AR-based surgical navigation system adaptable to various types of patient data.

In the proposed system, a fixed Young's modulus was adopted based on a previous study [26]. The Young's modulus of bone and soft tissues in the knee can vary substantially across patients depending on age, sex, pathology and measurement method. In particular, there is currently no widely accessible technique for accurately estimating patient-specific physical parameters solely from medical imaging modalities such as CT without tissue biopsy [39]. Therefore, in the context of the proposed system, patient-specific parameterization was not considered critical.

To mitigate such patient-specific variability, we introduced both bone and surface force into the deformation process. For the fixed Young's modulus, the magnitudes of these forces were empirically determined to ensure consistently high deformation accuracy toward the flexion state across all patient datasets. Notably, the surface force magnitude is dynamically adjusted according to the degree of alignment between the depth information and the association model. This dynamic adjustment compensates for differences in deformation behaviour caused by anatomical variability between patients. As a result, although the internal bone motion simulated by the association model may not exactly match the actual flexion process of a patient, the final deformed shape closely approximates the true knee bone position in the flexion state.

Currently, our system has been tested in a laboratory environment that was slightly dimmer than an actual operating room. However, since knee arthroscopy procedures are typically performed without additional external lighting and rely on internal illumination from the arthroscope, we believe that the ambient lighting difference does not substantially impact the RGBD camera's performance. In addition, in some frames during simulation, the bone model may appear outside the skin model. This effect can occur because the knee surface model is represented by hexahedral elements, meaning that the finite element model and the visualization model are not perfectly matched. In regions where the skin layer is thin, such as the femoral epicondyle, this mismatch can make the bone appear to protrude outside the surface even though it remains within the hexahedral elements. Therefore, to achieve a more accurate implementation of the dynamic anatomy model, we plan to refine the finite element representation of the surface.

Although the proposed system operates effectively in most cases, there are certain failure cases. The most critical issue arises from the limitation of the RGBD camera, which captures only one side of the knee surface. Although the predefined reference distance is used in surface force computation to prevent the opposite side of the knee surface model from being undesirably pulled toward the observed surface during deformation, this mechanism may fail if the quality of the initial registration is poor, leading to simulation failure. Another failure case occurs when the knee undergoes rapid or large movements. Since the current system operates at approximately 10 fps, it is unable to accurately track sudden large knee movements, which may also result in simulation failure.

To address these limitations, our future research will focus on developing an artificial intelligence-based method to reconstruct the complete knee shape from one-sided 3D depth information, thereby preventing surface force-related failure cases. In addition, we plan to improve real-time responsiveness for rapid knee motion by optimizing the FEM solver. Finally, we are planning to validate the proposed system under actual operating room conditions following further technical improvements.

The dynamic anatomy model developed for the knee can be extended to other joints as well. In shoulder arthroscopy, the bending angle of the joint is adjusted during surgery to facilitate instrument entry. Therefore, bone alignment differ from the preoperative image, requiring compensation for bone movement to ensure accurate AR visualization. The shoulder joint can also be simulated using an association model comprising joint bones and surfaces. The shoulder surface deformation can be measured using an RGBD camera, and moving the bones according to the surface deformation can allow for AR-based surgical navigation as well.

Author Contributions

Deokgi Jeung contributed to methodology design, software development and manuscript writing. Hyun-Joo Lee and Hee-June Kim were responsible for data acquisition, analysis and experimental validation. Hyunseok Choi supported software development and system implementation. Jaesung Hong supervised the overall research, contributed to methodology development and participated in manuscript writing and editing.

Acknowledgements

This work was supported by the National Research Foundation of Korea (NRF) grant funded by the Korea government (MSIT) (No. RS-2024-00355535) and the Digital Medical Products Development Based on Medical Data Synthesis and AI Technologies Program (RS-2025-02305698, Development of On-Device AI Digital Medical Products Utilizing

Synthetic Technology and Synthetic Data for Atypical Medical Data) funded by the Ministry of Trade, Industry & Energy (MOTIE) of Korea.

Conflicts of Interest

The authors declare no conflicts of interest.

Data Availability Statement

The data that support the findings of this study are available on request from the corresponding author. The data are not publicly available due to privacy or ethical restrictions.

References

1. M. J. Salzler, A. Lin, C. D. Miller, S. Herold, J. J. Irrgang, and C. D. Harner, "Complications After Arthroscopic Knee Surgery," *American Journal of Sports Medicine* 42, no. 2 (2013): 292–296.

2. P. B. Jorge, D. Escudeiro, N. R. Severino, et al., "Positioning of the Femoral Tunnel in Anterior Cruciate Ligament Reconstruction: Functional Anatomical Reconstruction," *BMJ Open Sport & Exercise Medicine* 4, no. 1 (2018): 5–8.

3. T. C. Keller, M. Tompkins, K. Economopoulos, et al., "Tibial Tunnel Placement Accuracy During Anterior Cruciate Ligament Reconstruction: Independent Femoral Versus Transtibial Femoral Tunnel Drilling Techniques," *Arthroscopy - Journal of Arthroscopic and Related Surgery* 30, no. 9 (2014): 1116–1123.

4. H. K. Haroun, M. M. Abouelsoud, M. R. Allam, and M. M. Abdelwahab, "Transtibial Versus Independent Femoral Tunnel Drilling Techniques for Anterior Cruciate Ligament Reconstruction: Evaluation of Femoral Aperture Positioning," *Journal of Orthopaedic Surgery and Research* 17, no. 1 (2022): 166.

5. M. J. M. Zee, P. A. J. Pijpker, J. Kraeima, A. R. Viddeleer, and R. L. Diercks, "Patient Specific Instrumentation in ACL Reconstruction: A Proof of Concept Cadaver Experiment Assessing Drilling Accuracy When Using 3D Printed Guides," *Archives of Orthopaedic and Trauma Surgery* 144 (2024): 289–296.

6. E. Inderhaug, A. Larsen, P. A. Waaler, T. Strand, T. Harlem, and E. Solheim, "The Effect of Intraoperative Fluoroscopy on the Accuracy of Femoral Tunnel Placement in Single-Bundle Anatomic ACL Reconstruction," *Knee Surgery, Sports Traumatology, Arthroscopy* 25, no. 4 (2017): 1211–1218.

7. K. Jung, H. Kim, E. Kholinne, et al., "Navigation-Assisted Anchor Insertion in Shoulder Arthroscopy: A Validity Study," *BMC Musculoskeletal Disorders* 21, no. 1 (2020): 1–8.

8. I. Micic, E. Kholinne, H. Hong, et al., "Navigation-Assisted Suture Anchor Insertion for Arthroscopic Rotator Cuff Repair," *BMC Musculoskeletal Disorders* 20, no. 1 (2019): 1–8.

9. J. M. Li, D. D. Bardana, and A. J. Stewart, "Augmented Virtuality for Arthroscopic Knee Surgery," *Medical Image Computing and Computer-Assisted Intervention* 14, no. Pt 1 (2011): 186–193.

10. A. W. L. Dickinson, M. L. Zec, D. R. Pichora, B. J. Rasquinha, and R. E. Ellis, "Electromagnetically Tracked Personalized Templates for Surgical Navigation," *International Journal of Computer Assisted Radiology and Surgery* 12, no. 6 (2017): 1049–1058.

11. W. Y. X. Foo, A. C. C. Chou, H. M. Lie, and D. T. T. Lie, "Computer-assisted Navigation in ACL Reconstruction Improves Anatomic Tunnel Placement With Similar Clinical Outcomes," *Knee* 38 (2022): 132–140.

12. S. Tsukada, H. Ogawa, K. Kurosaka, M. Saito, M. Nishino, and N. Hirasawa, "Augmented Reality-Aided Unicompartmental Knee Arthroplasty," *Journal of Experimental Orthopaedics* 9 (2022): 88.

13. C. Ma, X. Cui, F. Chen, L. Ma, S. Xin, and H. Liao, "Knee Arthroscopic Navigation Using Virtual-Vision Rendering and Self-Positioning Technology," *International Journal of Computer Assisted Radiology and Surgery* 15, no. 3 (2020): 467–477.

14. H. Shu, M. Liu, L. Seenivasan, et al., "Seamless Augmented Reality Integration in Arthroscopy: A Pipeline for Articular Reconstruction and Guidance," *Healthcare Technology Letters* 12, no. 1 (2025): 1–12.

15. J. Wang, J. Liu, L. Wu, et al., "Accuracy of Femoral Tunnel Localization With Mixed Reality Technology-Assisted Single-Bundle ACL Reconstruction," *Orthopaedic Journal of Sports Medicine* 11, no. 7 (2023): 23259671231184399.

16. F. Chen, X. Cui, B. Han, J. Liu, X. Zhang, and H. Liao, "Augmented Reality Navigation for Minimally Invasive Knee Surgery Using Enhanced Arthroscopy," *Computer Methods and Programs in Biomedicine* 201 (2021): 105952.

17. Ø. Bjelland, B. Rasheed, H. G. Schaathun, et al., "Toward a Digital Twin for Arthroscopic Knee Surgery: A Systematic Review," *IEEE Access* 10 (2022): 45029–45052.

18. I. Peterlík, C. Duriez, and S. Cotin, "Modeling and Real-Time Simulation of a Vascularized Liver Tissue," *Medical Image Computing and Computer-Assisted Intervention* 15, no. Pt 1 (2012): 50–57.

19. N. Haouchine, S. Cotin, I. Peterlik, et al., "Impact of Soft Tissue Heterogeneity on Augmented Reality for Liver Surgerye," *IEEE Transactions on Visualization and Computer Graphics* 21, no. 5 (2015): 584–597.

20. N. Golse, A. Petit, M. Lewin, E. Vibert, and S. Cotin, "Augmented Reality During Open Liver Surgery Using a Markerless Non-Rigid Registration System," *Journal of Gastrointestinal Surgery* 25, no. 3 (2021): 662–671.

21. A. Fedorov, R. Beichel, J. Kalpathy-Cramer, et al., "3D Slicer as an Image Computing Platform for the Quantitative Imaging Network," *Magnetic Resonance Imaging* 30, no. 9 (2012): 1323–1341.

22. M. Müller, J. Dorsey, L. McMillan, R. Jagnow, and B. Cutler, "Stable Real-Time Deformations," in *Proceedings of the Computer Animation Conference* (Association for Computing Machinery, 2002), 49–54.

23. M. Nesme, Y. Payan, and F. Faure, "Efficient, Physically Plausible Finite Elements," in *Eurographics* (Eurographics Association, 2005), 77–80.

24. O. Etzmuss, M. Keckeisen, and W. Strasser, "A Fast Finite Element Solution for Cloth Modelling," *Proceedings of the Pacific Conference on Computer Graphics and Applications* (IEEE, 2003), 244–251.

25. G. Irving, J. Teran, and R. Fedkiw, "Invertible Finite Elements for Robust Simulation of Large Deformation," in *Proceedings of the 2004 ACM SIGGRAPH / Eurographics Symposium on Computer Animation (SCA '04)* (Eurographics Association, 2004), 131–140.

26. A. D. Sylvester and P. A. Kramer, "Young's Modulus and Load Complexity: Modeling Their Effects on Proximal Femur Strain," *Anatomical Record* 301 (2018): 1189–1202.

27. M. Nesme, Y. Payan, and F. Faure, "Animating shapes at arbitrary resolution with non-uniform stiffness," in *Proceedings of the 3rd Workshop on Virtual Reality, Interactions, and Physical Simulation (VRIPHYS)* (Eurographics Association, 2006), 17–24.

28. A. Petit, S. Cotin, V. Lippiello, and B. Siciliano, "Capturing Deformations of Interacting Non-Rigid Objects Using RGB-d Data," in *IEEE International Conference on Intelligent Robots and Systems* (IEEE, 2018), 491–497.

29. P. J. Besl and N. D. McKay, "A Method for Registration of 3-D Shapes," *IEEE Transactions on Pattern Analysis and Machine Intelligence* 14 (1992): 239–256.

30. D. Jeung, K. Jung, H. J. Lee, and J. Hong, "Augmented Reality-Based Surgical Guidance for Wrist Arthroscopy With Bone-Shift Compensation," *Computer Methods and Programs in Biomedicine* 230 (2023): 107323.

31. S. Lee, S. Shim, H. G. Ha, H. Lee, and J. Hong, "Simultaneous Optimization of Patient-Image Registration and Hand-Eye Calibration for Accurate Augmented Reality in Surgery," *IEEE Transactions on Biomedical Engineering* 67 (2020): 2669–2682.

32. F. J. Romero-Ramirez, R. Muñoz-Salinas, and R. Medina-Carnicer, "Speeded up Detection of Squared Fiducial Markers," *Image and Vision Computing* 76 (2018): 38–47.

33. M. Stenmark, E. Omerbai, M. Magnusson, V. Andersson, M. Abrahamsson, and P.-K. Tran, "Vision-Based Tracking of Surgical Motion During Live Open-Heart Surgery," *Journal of Surgical Research* 271 (2022): 106–116.

34. J. Gibby, S. Cvetko, R. Javan, R. Parr, and W. Gibby, "Use of Augmented Reality for Image-Guided Spine Procedures," *European Spine Journal* 29, no. 8 (2020): 1823–1832.

35. F. Faure, D. H. Duriez, C. J. Allard, et al., "SOFA: A Multi-Model Framework for Interactive Physical Simulation," *Studies in Mechanobiology, Tissue Engineering and Biomaterials* 11 (2012): 283–321.

36. M. Servi, A. Profili, R. Furferi, and Y. Volpe, "Comparative Evaluation of Intel Realsense d415, d435i, d455, and Microsoft Azure Kinect DK Sensors for 3D Vision Applications," *IEEE Access* 12 (2024): 111311–111321.

37. K. Chung, C. H. Choi, S.-H. Kim, S.-J. Kim, W. Do, and M. Jung, "The Relationship Between Lateral Femoral Anatomic Structures and the Femoral Tunnel Outlet in Anterior Cruciate Ligament Reconstruction Using the Transportal Technique: A 3-Dimensional Simulation Analysis," *Orthopaedic Journal of Sports Medicine* 8, no. 9 (2020): 2325967120952783.

38. Z. Zhang, B. Meng, W. Li, and J. Cao, "The Role of Navigation Technology in Anterior Cruciate Ligament Reconstruction Bone Tunnel Positioning," *Journal of Robotic Surgery* 19, no. 1 (2025): 90.

39. P. O. Dmitriev, A. A. Golyadkina, L. V. Bessonov, I. I. Kirillova, L. Y. Kossovich, and A. S. Falkovich, "The Dependence of Young'S modulus of Trabecular Bony Tissue on Its Density According to Computed Tomography," in *Proceedings of the SPIE 11229, Advanced Biomedical and Clinical Diagnostic and Surgical Guidance Systems XVIII* (SPIE, 2020), 2545077.